This is an *Accepted Manuscript*, which has been through the Royal Society of Chemistry peer review process and has been accepted for publication.

Accepted Manuscripts are published online shortly after acceptance, before technical editing, formatting and proof reading. Using this free service, authors can make their results available to the community, in citable form, before we publish the edited article. We will replace this *Accepted Manuscript* with the edited and formatted *Advance Article* as soon as it is available.

You can find more information about *Accepted Manuscripts* in the **Information for Authors**.

Journal Name

Dynamic Article Links ▶

ARTICLE TYPE

Synthesis, crystal structure and luminescence properties of $Y_4Si_2O_7N_2$: Ce^{3+} phosphor for near-UV white LEDs

Quansheng Wu, Zhigang Yang, Zhengyan Zhao, Meidan Que, Xicheng Wang, and Yuhua Wang*

A near-UV excited phosphor $Y_4Si_2O_7N_2$: Ce^{3+} was synthesized using a solid-state reaction. The crystal structure and luminescence properties were studied. $Y_4Si_2O_7N_2$ crystallizes in a monoclinic unit cell with space group P21/c and lattice constants $a = 7.5678(2)$ Å, $b = 10.4529(1)$ Å, $c = 10.7779(3)$ Å, $\beta = 110.06$ º, and cell volume = 800.85(2) Å^3. The crystal structure of $Y_4Si_2O_7N_2$ showing the $Si(O,N)_4$ polyhedron is
10 given and there are four different coordination environments of Y^{3+} with two different coordination numbers in the structure of $Y_4Si_2O_7N_2$. Ce^{3+}-doped $Y_4Si_2O_7N_2$ exhibited a broad emission band and the maximum emission wavelength could be tuned from blue ($\lambda_{em} = 450$ nm) to green ($\lambda_{em} = 515$ nm) by increasing the concentration of Ce^{3+}. The quantum efficiency was determined to be about 47%. The results present $Y_4Si_2O_7N_2$: Ce^{3+} as a candidate for use as a conversion phosphor for near-UV white LED
15 applications.

1. Introduction

In recent years, there has been a growing focus on research in the area of white light-emitting-diodes (LEDs) due to their merits of
20 being environmentally friendly, highly efficient and having a longer lifetime.[1–6] Hence, white LEDs are expected to be a promising candidate to replace conventional incandescent and fluorescent lamps. Typically, white light can be generated by blue LED chips and the yellow phosphor YAG: Ce^{3+} (YAG).[7]
25 However, the disadvantages of this combination are low color-rendering index and high color temperature due to the deficiency of red emission in the visible spectrum. Accordingly, during the past few years, the white LEDs fabricated using near-ultraviolet (n-UV) LEDs (380–420 nm) coupled with red, green, and blue
30 phosphors have attracted much attention. This technology has a higher CRI and high tolerance to the UV chip's color variation.[8, 9] Hence, there is an urgent need to develop new n-UV excitable phosphors. Among those phosphors used to combine with the n-UV LEDs, nitride/oxynitride hosts are good candidates as host
35 lattices for phosphors due to several merits, such as high chemical stability and good thermal quenching, and exhibit intense luminescence for white LEDs application when activated with Ce^{3+}/Eu^{2+}, such as in $M_2Si_5N_8$ (M = Ca, Sr, Ba), Ca-α-SiAlON, γ-AlON and so on.[10–17]
40 In the Y–Si–O–N quaternary system，there are five crystalline phases that have been identified and studied: $Y_2Si_3O_3N_4$, $Y_4Si_2O_7N_2$, $Y_5Si_3O_{12}N$, $YSiO_2N$, and $Y_3Si_5N_9O$.[18, 19] These compounds are always needing critical synthesis conditions, such as high temperature and high pressure. Moreover, the structures
45 of the Y–Si–O–N compounds have not been completely identified and studied; which limited interest has been paid to the

photoluminescence (PL) properties.[20–23] Although Zhiguo Xia et al.[24] reported the preparation and luminescent properties of $Y_4Si_2O_7N_2$, they did not obtain the pure phase of $Y_4Si_2O_7N_2$.
50 Furthermore, they did not investigative the crystal structure of $Y_4Si_2O_7N_2$ and the relation of crystal structure with the luminescent properties.
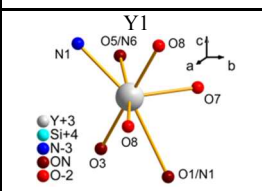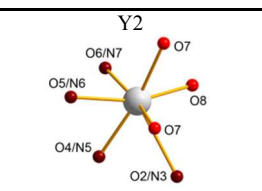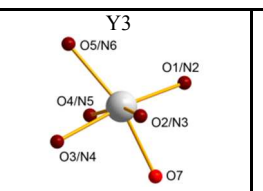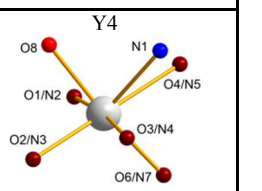Therefore, in order to better for the basic research and explore the potential applications in n-UV LEDs, in this paper, we
55 synthesized a series of Ce^{3+} doped $Y_4Si_2O_7N_2$: xCe^{3+} (x = 0–10 mol%) pure phase via high temperature solid-state reaction. We refined the crystal structure of $Y_4Si_2O_7N_2$: Ce^{3+} and studied the PL properties of the $Y_4Si_2O_7N_2$: Ce^{3+} phosphors, which exhibited tunable emission color from blue to green under n-UV light
60 excitation. These results demonstrated that $Y_4Si_2O_7N_2$: Ce^{3+} is a promising phosphor for n-UV white LEDs.

2. Experimental

A series samples of $Y_4Si_2O_7N_2$: xCe^{3+} (0 ≤ x ≤ 10 mol%) were prepared by conventional solid-state reaction. Stoichiometric
65 amounts of powder Si_3N_4 (99.9%), Y_2O_3 (99.99%), CeO_2 (99.99%) and H_3BO_3 were ground in an agate mortar and then sintered at 1600 ℃ for 2 h under NH_3/N_2 gas flow. H_3BO_3 was used as a flux.
The phase purity was determined by a X-ray diffractometer
70 (XRD, Rigaku D/Max-2400) at a scanning rate of 2° min^{-1} and intervals of 0.02° in the 2θ range from 10° to 110° with Cu Kα radiation ($\lambda = 1.5405$ Å). The crystal structure was refined by the Rietveld method using the Maud (Materials Analysis Using Diffraction) program.[25] The morphology of the sample was
75 examined using scanning electron microscopy (SEM, Hitachi-4800) and transmission electron microscopy (TEM, FEI Tecnai

Table 1 The Y-N (O) bond length data along with a schematic polyhedral for each Y site.

Distance less than 2.8 (Å)			
Y1	Y2	Y3	Y4
Y1-N1: 2.3293(2)	Y2-O2/N3: 2.6965(3)	Y3-O1/N2: 2.3130(4)	Y4-N1: 2.4839(2)
Y1-O1/N2: 2.7709(3)	Y2-O4/N5: 2.3091(3)	Y3-O2/N3: 2.2731(4)	Y4-O1/N2: 2.3179(4)
Y1-O3/N4: 2.4219(3)	Y2-O5/N6: 2.2848(3)	Y3-O3/N4: 2.2634(3)	Y4-O2/N3: 2.3866(4)
Y1-O5/N6: 2.6959(3)	Y2-O6/N7: 2.3022(3)	Y3-O4/N5: 2.3379(3)	Y4-O3/N4: 2.5917(3)
Y1-O7: 2.3168(5)	Y2-O7: 2.2724(4)	Y3-O5/N6: 2.3656(3)	Y4-O4/N5: 2.5996(3)
Y1-O8: 2.2438(3)	Y2-O7: 2.3018(5)	Y3-O7: 2.2245(4)	Y4-O6/N7: 2.3012(2)
Y1-O8: 2.2654(4)	Y2-O8: 2.1622(3)	Average: 2.2962(8)	Y4-O8: 2.2889(3)
Average: 2.4348(9)	Average: 2.3327(4)		Average: 2.4242(8)

F30, operated at 300 kV). The crystal structures were analyzed by.high-resolution transmission electron microscopy (HRTEM, FEI Tecnai F30, operated at 300 kV). The element composition was determined using an energy-dispersive X-ray spectroscopy (EDX) which was attached to the TEM. Reflectance spectra were measued on UV-vis spectrophotometer (PE lambda950). The photoluminescence (PL) and photoluminescence excitation (PLE) spectra of the samples were measured by using the fluorescence spectrophotometer (FLS-920T) equipped with a 450W Xe light source and double excitation monochromators. The quantum efficiency (QE) was measured by the spectrofluorometer (HORIBA JOBIN YVON Fluorlog-3) equipped with 450W xenon lamp. The temperature-dependent luminescence measurements were also carried out by the HORIBA JOBIN YVON Fluorlog-3 spectrofluorometer system starting from 20 ℃ to 200 ℃ in steps of about 30 ℃ with a hearing rate of 20 ℃/min. The PL decay curves were measured by an FLS-920T fluorescence spectrophotometer with nF900 nanosecond Flashlamp as the light source.
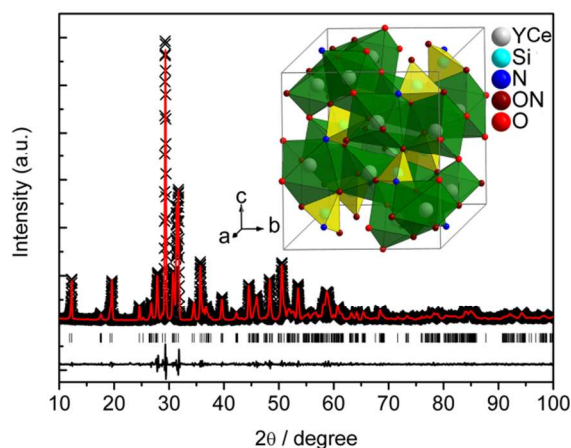
3. Results and discussion

Fig. 1 Observed (crosses), calculated (solid line), and difference (bottom) XRD profiles for the Rietveld refinement of $Y_4Si_2O_7N_2$:2%Ce^{3+}. Bragg reflections are indicated with tick marks.

Fig. 1 shows the Rietveld refinement of $Y_4Si_2O_7N_2$: 2 mol%Ce^{3+} phosphor. All of the observed XRD peaks are obtained with goodness of fit parameters Rw = 7.60%, $Rwmb$ = 5.75% and sig = 1.21. These results indicate that when doped with 2 mol% Ce^{3+} per mol Y^{3+}, the $Y_4Si_2O_7N_2$ host is a single-phase structure. $Y_4Si_2O_7N_2$: 2 mol%Ce^{3+} crystallizes in a monoclinic unit cell with space group P21/c and lattice constants a = 7.5678(2) Å, b = 10.4529(1) Å, c= 10.7779(3) Å, β = 110.06 º, and cell volume = 800.85(2) $Å^3$. As shown in Table 1, the Y^{3+} ions have four different sites in a unit cell. Y(1), Y(2) and Y(4) are defined as being seven-coordinated; Y(3) are defined as being six-coordinated. Among them, Y(1) and Y(2) sites are surrounded by three free oxygen ions and the other sites Y(3) and Y(4) are surrounded by one free oxygen ions. Every Y site in $Y_4Si_2O_7N_2$ has Wyckoff symbol 4e (site symmetry C_1). The ionic radii for six- and seven-coordinated Y^{3+} are 0.90 and 0.96 Å, respectively. The ionic radii for six- and seven-coordinated Ce^{3+} are 1.01 and 1.07 Å, respectively. On account of the matching of ionic radii and the charge balance, the Ce^{3+} ions could randomly occupy the Y^{3+} ions sites in the $Y_4Si_2O_7N_2$ host. Accordingly, different emission centers originated from the different sites will be formed.
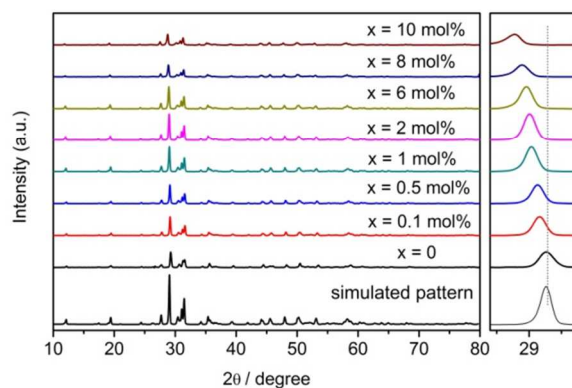

Fig. 2 X-ray diffraction patterns of $Y_4Si_2O_7N_2$:xCe^{3+} (0 ≤ x ≤ 10%).
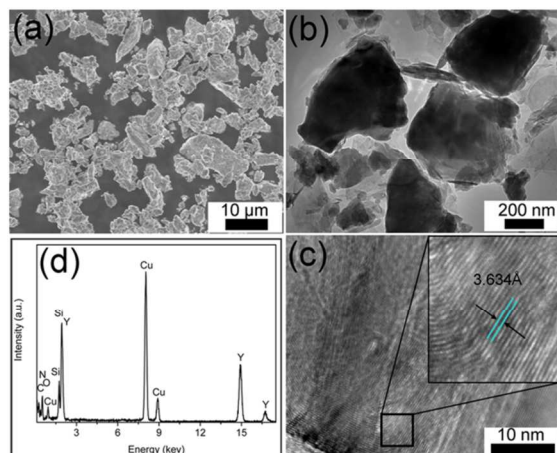
Fig. 3 (a) SEM image, (b) TEM image, (c) HRTEM image and EDX spectrum of $Y_4Si_2O_7N_2$:2%Ce^{3+}.

For $Y_4Si_2O_7N_2$: xCe^{3+} ($0 \leq x \leq 10$ mol%), all diffraction patterns matched well with the simulated pattern, as shown in Fig. 2. This indicates the monophasic $Y_4Si_2O_7N_2$-based phosphors were prepared. The diffraction peaks of $Y_4Si_2O_7N_2$: xCe^{3+} ($0 \leq x \leq 10$ mol%) are shifted a little to lower angles with respect to the position of standard $Y_4Si_2O_7N_2$. This is because the radius of Ce^{3+} is bigger than that of Y^{3+} in the $Y_4Si_2O_7N_2$ host lattice, showing that Ce^{3+} has been effectively built into $Y_4Si_2O_7N_2$ host lattice. The lattice constants of $Y_4Si_2O_7N_2$:$xCe^{3+}$are summarized in Table 2. The lattice constants become larger with increasing the Ce^{3+}doping concentrations, which consistent with the shift of diffraction peaks. The typical SEM image of $Y_4Si_2O_7N_2$: 2 mol%Ce^{3+} is given in Fig. 3(a). The obtained powders are well-dispersed. The typical low-magnification TEM images and HRTEM image are shown in Fig. 3(b) and (c), respectively. The interplanar spacing was measured to be 3.634 Å, which matchs well with the (022) interplanar distance of monoclinic $Y_4Si_2O_7N_2$. These results show that well-crystallized $Y_4Si_2O_7N_2$:Ce^{3+} powders have been obtained. The corresponding EDX spectrum analysis (Fig. 3(d)) indicates that the product has a chemical composition of Y, Si, O, N, and no impurity element exists.

Table 2. Lattice constants of $Y_4Si_2O_7N_2$:xCe^{3+}

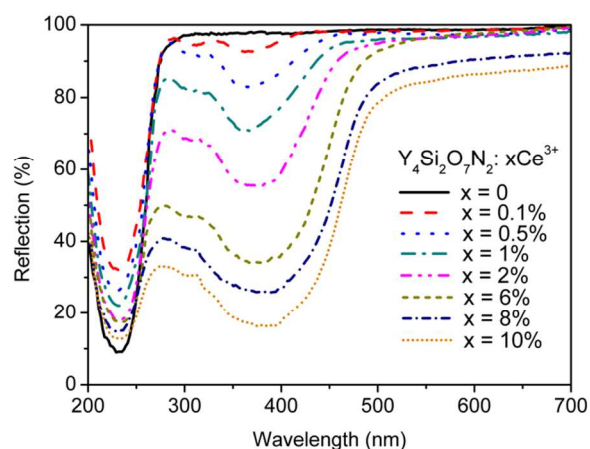|	a (Å)	b(Å)	c(Å)	β(°)	v(Å³)
X=0	7.5499(2)	10.4365(1)	10.7663(1)	110.04	796.96(6)
X=2%	7.5678(2)	10.4529(1)	10.7779(3)	110.06	800.85(2)
X=6%	7.5716(1)	10.4639(2)	10.7825(4)	110.21	801.69(0)
X=10%	7.5836(2)	10.4739(2)	10.7920(2)	110.61	802.34(8)

Fig. 4 Reflection spectra of $Y_4Si_2O_7N_2$:xCe^{3+} ($0 \leq x \leq 10\%$).

Reflection spectra are recorded for the undoped host and Ce^{3+}-doped $Y_4Si_2O_7N_2$ (Fig. 4). The strong absorption in the range of 200–250 nm of the undoped sample, which with white body color, is due to the host absorption. Accordingly, the absorption edge of the undoped sample was estimated to be 244 nm (5.08 eV). For the Ce^{3+}-doped samples, strong absorption bands are presented from 250 to 450 nm region, which is assigned to $4f^1 \rightarrow 4f^05d^1$ transition of Ce^{3+} ion. With increasing Ce^{3+} concentration, the absorption becomes stronger and the absorption edges shift to the longer wavelength portion, which yields the body color of phosphors varying from white to pale yellow.
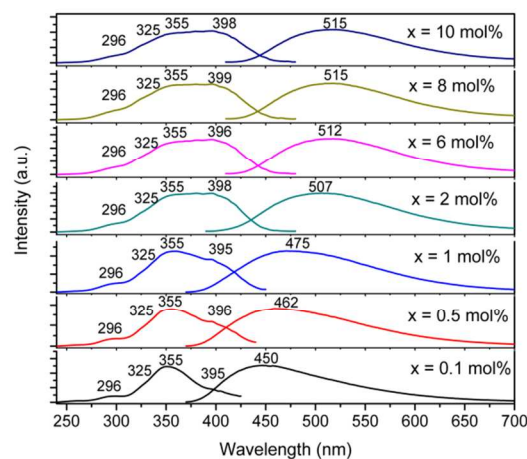

Fig. 5 Excitation and emission spectra of $Y_4Si_2O_7N_2$:Ce^{3+} with varying Ce^{3+} concentrations(λ_{ex}=355nm).
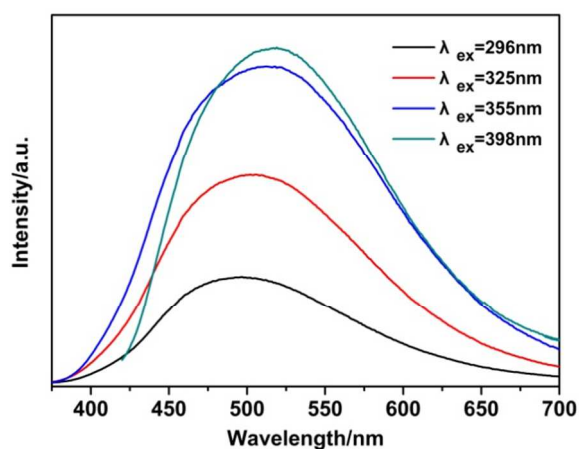
Fig. 6 emission spectra of $Y_4Si_2O_7N_2$:2%Ce^{3+} with varying excitation.

Fig. 5 shows the excitation and emission spectra of $Y_4Si_2O_7N_2$: Ce^{3+} for different Ce^{3+} concentrations. The excitation bands of the samples doped with varying concentrations of Ce^{3+} had peaks at ~296 nm, ~325 nm, ~355 nm, and ~395 nm, respectively, corresponding to the transition from the Ce^{3+} $4f^1$ ground state to the lowest $5d$ splitting level. According to the series of excitation spectra, the samples could be efficiently excited in the range of 355–410 nm, which was consistent with the reflectance spectra of $Y_4Si_2O_7N_2$: Ce^{3+} shown in Fig. 4. Consequently, this phosphor could be efficiently excited by the n-UV LED chips. A broad and asymmetric band in the wide wavelength range from 400 to 650 nm was observed in emission spectra, which originated from $5d \rightarrow 4f$ transition. The broad emission band was attributed to the high covalency of the Ce–N bond and a large crystal-field splitting effect. The crystal-field splitting of Ce^{3+} shown in Table 4 were estimated to be 8467-8721 cm^{-1} in $Y_4Si_2O_7N_2$. Although four different sites for Y exist in $Y_4Si_2O_7N_2$, the shapes of emission spectra did not change greatly with varying excitation wavelengths, as shown in Fig.6, indicating a strong spectral overlap between spectra belonging to different luminescent centers.
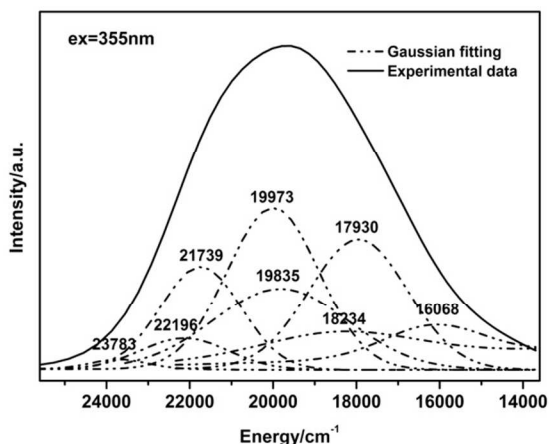

Fig. 7 Gaussian fitting of the emission band of $Y_4Si_2O_7N_2$:2%Ce^{3+}.

The emission band of $Y_4Si_2O_7N_2$:2% Ce^{3+} is decomposed into eight well-separated Gaussian components (in Fig.7) with maxima at 23783 cm^{-1} (420 nm), 22196 cm^{-1} (451 nm), 21739 cm^{-1} (460 nm), 19973 cm^{-1} (501 nm), 19835 cm^{-1} (504 nm), 18234 cm^{-1} (548 nm), 17930 cm^{-1} (558 nm), and 16068 cm^{-1} (622

nm), respectively. It is accepted that the emission of Ce^{3+} can be attributed to the transitions from the lowest 5d excited state to the $^2F_{5/2}$ and $^2F_{7/2}$ ground state, so that two distinguished emission spectra with the theoretical energy value of 2000 cm^{-1} can be decomposed. The above values can be divided into four groups according to the calculated Gaussian energy values, which verified that Ce^{3+} will occupy different Y^{3+} centers in the present $Y_4Si_2O_7N_2$ host. The position of the emission peak is highly dependent on the crystal-field strength of the activators. The relation between the crystal-field strength (D_q) and R is expressed as the following equation:[26]

$$D_q = \frac{3Ze^2r^4}{5R^5} \qquad (1)$$

Where Z is the charge of valence of the anion, R represents the distance between the central ion and its ligands, and r is the mean size of a center ion. It can be seen from the equation that D_q is inversely proportional to the fifth power of the bond length R. Because the average Ce_Y—N/O distance is longer for $Ce_{Y1, 2, 4}$—N/O than that for Ce_{Y3}—N (as seen in Table I), the crystal-field strength of Ce^{3+} at Y(3) sites is larger than that at Y(1, 2, 4) sites. Accordingly, the splitting of the 5d levels of Ce^{3+} at Y(3) sites is larger than that at Y(1, 2, 4) sites. Therefore, the lowest excited state of Ce^{3+} at Y(3) sites is lower in energy than that at Y(1, 2, 4) sites. Hence, it can be deduced that the lowest-energy (622nm and 548nm) peaks was assigned to the transitions of Ce^{3+} ions occupied at Y(3)sites. Moreover, J.W.H. van Krevel[27] studied the ordering of nitrogen and oxygen in $Y_4Si_2O_7N_2$ by Neutron diffraction, indicating that Y(2) is the most oxygen-rich coordination(YO7 or YO6N) and Y(4) is the most nitrogen-rich coordination(YO5N2). So it can be deduced that the 558nm and 504nm, 501nm and 451nm, and 460nm and 420nm peaks were assigned to the transitions of Ce^{3+} ions occupied at Y(4), Y(1) and Y(2) sites, respectively.

To further understand that Ce^{3+} ions occupy different 4 sites, the PL decay curves of the Ce^{3+} in $Y_4Si_2O_7N_2$:2%Ce^{3+} were obtained with an excitation at 355 nm and monitored at 461 nm, 500nm, 550nm and 632nm, respectively, as shown in Fig. 8.

It can be seen that the varied decay curves of Ce^{3+} ions upon 355 nm excitation can be fitted well with order exponential decay curve using the following equation.[28,29]

$$I = A_1 \exp\left(\frac{-t}{\tau_1}\right) + A_2 \exp\left(\frac{-t}{\tau_2}\right) + A_3 \exp\left(\frac{-t}{\tau_3}\right) + A_4 \exp\left(\frac{-t}{\tau_4}\right) \qquad (2)$$

where I is the luminescence intensity, A_1, A_2, A_3 and A_4 are constants,τ_1, τ_2, τ_3, and τ_4 are the four exponential components of the decay time. Using these parameters,

Table 3. The Measured Values of τ_1, τ_2, τ_3, τ_4, A_1, A_2, A_3 and A_4 of $Y_4Si_2O_7N_2$:2%Ce^{3+} Sample

	A_1	A_2	A_3	A_4	τ_1 (ns)	τ_2 (ns)	τ_3 (ns)	τ_4 (ns)	τ^*(ns)
λ_{em}=461nm	0.110	0.082	0.069	0.005	2.37	10.31	29.78	71.76	27.35
λ_{em}=500nm	0.058	0.051	0.067	0.036	1.78	8.11	23.20	50.10	33.54
λ_{em}=550nm	0.050	0.059	0.071	0.027	1.79	9.03	29.71	59.54	37.59
λ_{em}=632nm	0.066	0.056	0.063	0.022	1.90	9.34	30.47	63.36	38.35

the average decay time (τ^*) can be determined using the following formula[30]:

$$\tau^* = \frac{A_1\tau_1^2 + A_2\tau_2^2 + A_3\tau_3^2 + A_4\tau_4^2}{A_1\tau_1 + A_2\tau_2 + A_3\tau_3 + A_4\tau_4} \qquad (3)$$

The values of A_1, A_2, A_3, A_4, τ_1, τ_2, τ_3, τ_4 and τ^* are analyzed, determined, and summarized in Table 3. Each decay curve of $Y_4Si_2O_7N_2$:2%Ce^{3+} monitored at 461 nm, 500nm, 550nm and 632nm can be fitted to four exponential components. Moreover, the average decay times (τ^*) of $Y_4Si_2O_7N_2$:2%Ce^{3+} monitored at 461 nm, 500nm, 550nm and 632nm are different with each other. Thus, it can be substantiated that there are four different sites in $Y_4Si_2O_7N_2$.
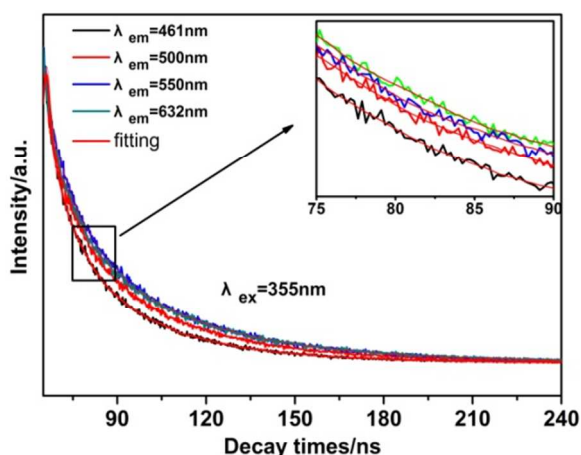

Fig. 8 PL decay curves of $Y_4Si_2O_7N_2$:2%Ce^{3+} monitored at 461nm, 500nm, 550 nm, 632nm，respectively.
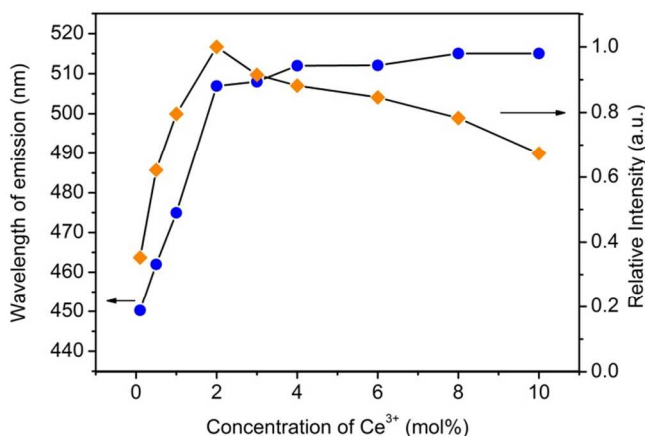

Fig. 9 Red shift of the peak position and the dependence of the emission intensity on the Ce^{3+} concentration from the spectra plotted in Fig. 5.

The dependence of the peak position and emission intensity of $Y_4Si_2O_7N_2$: Ce^{3+} on the Ce^{3+} content is shown in Fig. 9. With increasing Ce^{3+} content, the emission intensity is maximized at x = 2 mol%, and then decreases due to the concentration quenching effect. The concentration quenching is due to the non-radiative energy transfer among Ce^{3+} ions. Two mechanisms are adopted to explain the non-radiative energy transfer: multipolar interaction and radiation reabsorption. Because the luminescence originates from the allowed $4f^1 \rightarrow 4f^0 5d^1$ transition of the Ce^{3+} ion, the energy transfer process should be dominated by an electric multipolar interaction, as suggested by Blasse.[31] As shown in Fig. 5, the excitation and emission spectra overlap to some extent, indicating that the radiation reabsorption mechanism may also play a role in energy transfer of Ce^{3+}-doped $Y_4Si_2O_7N_2$ phosphors. The increase of Ce^{3+} concentration in the host lattice should result in smaller distances among the Ce^{3+} ions, which should increase the probability of energy transfer among the activator ions.[32] Thereafter the emission intensity is quenched for the higher Ce^{3+} concentration samples.

Table 4. Emission, stokes shift, crystal filed splitting and the CIE coordinates for $Y_4Si_2O_7N_2$:Ce^{3+}.

Samples	λ_{em} (nm)	Stokes shift (cm^{-1})	Crystal field splitting (cm^{-1})	CIE(x, y)
x = 0.1%	450	5947	8467	(0.21, 0.24)
x = 0.5%	462	6524	8531	(0.23, 0.28)
x = 1%	475	7116	8467	(0.24, 0.31)
x = 2%	507	8445	8658	(0.28, 0.39)
x = 6%	512	8638	8531	(0.30, 0.43)
x = 8%	515	8752	8721	(0.30, 0.44)
x = 10%	515	8752	8658	(0.31, 0.45)

Simultaneously, the peak position of $Y_4Si_2O_7N_2$: Ce^{3+} phosphors shifts from 450 to 515 nm by increasing the Ce^{3+} ion content up to 10 mol%. The red-shifting behavior is attributed to two factors: crystal field splitting and radiation re-absorption of the high energy emission. One of the featuring characteristics for the increase of the crystal field splitting is the change of the excitation band in shape and position. As depicted in Fig. 5, the excitation bands get broadened and extend to the longer wavelength part with increasing Ce^{3+} content. The emission, stokes shift, crystal filed splitting and the CIE coordinates for $Y_4Si_2O_7N_2$: xCe^{3+} are shown in Table 4. The stokes shifts and

crystal-field splittings were estimated to be 5947~8752 cm^{-1} and 8467-8721 cm^{-1}, respectively. The more Ce^{3+} atoms doped in the lattice lead to an increase of the crystal field splitting.[33–36] The increasing crystal field splitting lowers the lowest $5d$ splitting energy and the excitation and emission energy is lowered. As a result, the emission shifts to longer wavelength. Furthermore, the extension of the excitation spectra of the higher Ce^{3+} doping samples result in the reabsorption of the high energy emission, which could lead to a fairly longer wavelength.
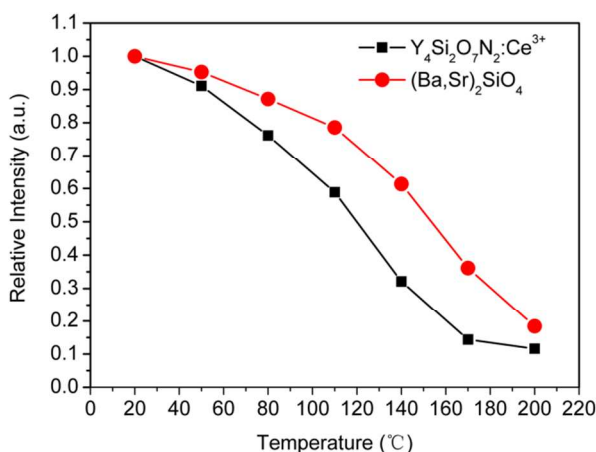

Fig.10 Thermal quenching data of Y$_4$Si$_2$O$_7$N$_2$:2 mol%Ce^{3+} excited at 395 nm. (Ba,Sr)$_2$SiO$_4$ was also measured as a reference.

Fig. 10 plots the relative emission intensity of Y$_4$Si$_2$O$_7$N$_2$:Ce^{3+} as a function of temperature using the green-emitting (Ba,Sr)$_2$SiO$_4$:Eu^{2+} commodity as a benchmark. The quenching temperature T_q (the temperature at which the emission intensity is half of the initial intensity at room temperature ~25 ℃) is about 120 ℃. We observed that the thermal stability of Y$_4$Si$_2$O$_7$N$_2$:Ce^{3+} was a little inferior to that of the green commodity phosphor. This phenomenon could be ascribed to the thermally active phonon-assisted tunneling from the excited states of lower-energy emission band to those of higher-energy emission band in the configuration coordinate diagram.[37]
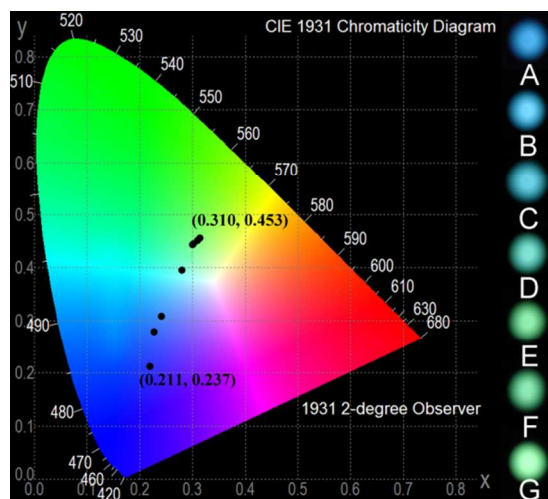

Fig. 11 CIE chromaticity coordinates and luminescence photographs under 365 nm irradiation of Y$_4$Si$_2$O$_7$N$_2$:xCe^{3+} phosphors with x = 0.1 (A), 0.5 (B), 1 (C), 2 (D), 6 (E), 8 (F) and 10 (G) mol%.

The Commission International de I′Eclairage (CIE) chromaticity coordinates and the photos for Y$_4$Si$_2$O$_7$N$_2$:Ce^{3+} phosphors with different Ce^{3+} dopant contents are shown in Fig. 11. The emission of Y$_4$Si$_2$O$_7$N$_2$:xCe^{3+} phosphors changed from blue at 450 nm to green at 515 nm with an increase in the x value and the CIE coordinates varies systematically from (0.21, 0.24) for the composition with 0.1 mol% (A) to (0.31, 0.45) for the composition with 10 mol% (G). The QE value of optimal sample with x = 2 mol% is determined to be about 47%. The corresponding photographs of the samples varied gradually from blue to green under 365 nm irradiation. It is indicated that controlling the activator concentrations can effectively shift the emitting colors of Y$_4$Si$_2$O$_7$N$_2$:Ce^{3+} phosphors.

4. Conclusions

In summary, we have synthesized a series single samples of Y$_4$Si$_2$O$_7$N$_2$:xCe^{3+} (0 ≤ x ≤ 10 mol%) via conventional solid-state reaction and reported the crystal structure and luminescent properties. The Y^{3+} ions have four different sites in a unit cell. Y(1), Y(2) and Y(4) are defined as being seven-coordinated; Y(3) are defined as being six-coordinated. The excitation spectra match well with the emission of UV LED chips (355–410 nm). A broad band in the wide wavelength range from 400 to 650 nm was observed in emission spectra (decomposed into four well-separated Gaussian components). This is due to the variation in the crystal-field strength around the activators. The emission spectra can be controlled with regards to the position (from blue to green) and intensity (maximum intensity was obtained for x = 2mol% and the QE is about 47%) over increasing Ce^{3+} content. These phosphors have the potential applications in n-UV chip pumped LEDs.

Acknowledgments

Notes and references

Key Laboratory for Special Function Materials and Structural Design of the Ministry of the Education, School of Physical Science and Technology, Lanzhou University, Lanzhou, 730000, China
Tel.: +86-931-8912772 (office); Fax: +86-931-8913554 (office); E-mail: wyh@lzu.edu.cn

1. Im WB, Kim YI, Fellows NN, Masui H, Hirata GA, DenBaars SP and Seshadri R, *Appl Phys Lett,* 2008, **93**, 091905-091907.
2. Nishida T, Ban T and Kobayashi N, *Appl Phys Lett,* 2003, **82**, 3817-3819.
3. Kim JS, Jeon PE, Choi JC, Park HL, Mho SI and Kim GG, *Appl Phys Lett,* 2004, **84**, 2931-2933.
4. Li XF, Budai J, Liu F, Howe J, Zhang JH, Wang XJ, Gu ZJ, Sun CJ, Meltzer RS, Pan ZW, *Light: Science & Applications,* 2013, **2**, e50.
5. Dai P P, Zhang XT, Bian LL, Lu S, Liu YC, and Wang XJ, *J Mater Chem C* 2013 **1**, 4570-6.
6. Hao ZD, Zhang JH, Zhang X, Sun XY, Luo YS, Lu SZ, and Wang XJ, *Appl Phys Lett,* 2007, **90**, 261113.

7. Lee S and Seo SY, *J Electrochem Soc*, 2002, **149**, J85-J88.
8. Kim JS, Jeon PE, Park YH, Choi JC, Park HL, Kim GC and Kim TW, *Appl Phys Lett*, 2004, **85**, 3696-3698.
9. Smet PF, Parmentier AB and Poelman D, *J Electrochem Soc*, 2011, **158**, R37-R54.
10. Li YQ, De With G and Hintzen HT, *J. Lumin.*, 2006, **116**, 107-116.
11. Mao ZY, Zhu YC, Gan L, Xu FF, Wang Y and Wang DJ, *J. Mate.r Chem.*, 2012, **22**, 824-826.
12. Shioi K, Hirosaki N, Xie RJ, Takeda T and Li YQ, *J. Mater. Sci.*, 2008, **43**, 5659-5661.
13. Shioi K, Hirosaki N, Xie RJ, Takeda T and Li YQ, *J. Mater. Sci.*, 2010, **45**, 3198-3203.
14. Zhang F, Chen S, Chen JF, Zhang HL, Li J, Liu XJ, Wang SW, *J. Appl. Phys.*, 2012, **111**, 083532-083535.
15. Liu WR, Yeh CW, Huang CH, Lin CC, Chiu YC, Yeh YT and Liu RS, *J. Mater. Chem.*, 2011, **21**, 3740-3744.
16. Tang JY, Xie WJ, Huang K, Hao LY, Xu X and Xie R, *J. Electrochem Solid-State Lett.*, 2011, **14**, J45-J47.
17. Wang XM, Wang CH, Kuang XJ, Zou RQ, Wang YX and Jing XP, *Inorg. Chem.*, 2012, **51**, 3540-3547.
18. MacKenzie KJD, Gainsford GJ and Ryan MJ, *J. Europ. Cerum. Soc.*, 1996, **16**, 553-560.
19. Wang JY, Zhou YC, Lin ZJ and Ohno T, *Phys. Rev. B*, 2008, **77**, 104117-104121.
20. Van Krevel JWH, Hintzen HT, Metselaar R and Meijerink A, *J. Alloys. Compd.*, 1998, **268**, 272-277.
21. Yang HC, Liu Y, Ye S and Qiu JR, *Chem. Phys. Lett.*, 2008, **451**, 218-221.
22. Deng DG, Xu SQ, Su XY, Wang Q, Li YQ, Li GF, Hua YJ, Huang LH, Zhao SL, Wang HP and Li CX, *Mater. Lett.*, 2011, **65**, 1176-1178.
23. Lu FC, Guo SQ, Yang ZP, Yang YM, Li PL, Li X, Liu QL (2012) J. Alloys. Compd. 521:77-82.
24. Xia ZG, Wu WW *Dalton Trans.*, 2013, **42**, 12989-12997.
25. Lutterotti L and Gialanella S, *Acta. Mater.*, 1998, **46**, 101-110.
26. W. B. Im, Y. I. Kim, N. N. Fellows, H. Masui, G. A. Hirata, S. P. Denbaar and R. Seshadri, *Appl. Phys. Lett.*, 2008, **93**, 091905.
27. Krevel J.W.H. van, on new rare-earth doped M-Si-Al-O-N materials luminescence properties and oxidation resistance, *Proefchrift*, 2000.
28. M. Yu, J. Lin and J. Fang, *Chem. Mater.*, 2005, **17**, 1783–91.
29. T. Moon, G. Y. Hong, H.-C. Lee, E.-A. Moon, B. W. Jeoung, S.-T. Hwang, J. S. Kim, and B.-G. Ryu, *Electrochem. Solid-State Lett.*, 2009, **12**, J61–3.
30. G. Blasse and B. C. Grabmaier, *Luminescent Materials.*, Springer, Berlin,1994.
31. Blasse G, *Phil. Res. Rep.*,1969, **24**, 131.
32. Sakuma K, Hirosaki N and Xie RJ, *J. Lumin.*, 2007, **126**, 843-852.
33. Höppe HA, Lutz H, Morys P, Schnick W, Seilmeier A, *J. Phys. Chem. Solids.*, 2000, **61**, 2001-2006.
34. Van Krevel JWH, Van Rutten JWT, Mandal H, Hintzen HTa nd Metselaar R, *J. Solid State Chem.*, 2002, **165**, 19-24.
35. Xie RJ, Hirosaki N, Mitomo M, Yamamoto Y and Suehiro T, *J. Phys. Chem. B*, 2004, **108**, 12027-12031.
36. Xie RJ, Hirosaki N, Suehiro T, Xu FF and Mitomo M, *Chem. Mater.*, 2006, **18**, 5578-5583.
37. Blasse G, Wanmalcer WL, Ter Vrygt GW and Bril A, *Phil. Res. Rep.*, 1968, **23**, 189.